LA-UR-15-27276 (Accepted Manuscript)

The Sedov Blast Wave as a Radial Piston Verification Test

Morgan, Nathaniel Ray
Pederson, Clark
Brown, Bart

Provided by the author(s) and the Los Alamos National Laboratory (2017-01-03).

To be published in: Journal of Verification, Validation and Uncertainty Quantification

DOI to publisher's version: 10.1115/1.4033652

Permalink to record: http://permalink.lanl.gov/object/view?what=info:lanl-repo/lareport/LA-UR-15-27276

Disclaimer:
Approved for public release. Los Alamos National Laboratory, an affirmative action/equal opportunity employer, is operated by the Los Alamos National Security, LLC for the National Nuclear Security Administration of the U.S. Department of Energy under contract DE-AC52-06NA25396. Los Alamos National Laboratory strongly supports academic freedom and a researcher's right to publish; as an institution, however, the Laboratory does not endorse the viewpoint of a publication or guarantee its technical correctness.

The Sedov Blast Wave as a Radial Piston Verification Test

Clark Pederson
XCP-Computational Physics Division,
Los Alamos National Laboratory
Los Alamos, New Mexico, 87545

Bart Brown
XCP-Computational Physics Division,
Los Alamos National Laboratory
Los Alamos, New Mexico, 87545

Nathaniel Morgan*
XCP-Computational Physics Division,
Los Alamos National Laboratory
Los Alamos, New Mexico, 87545

The Sedov blast wave is of great utility as a verification problem for hydrodynamic methods. The typical implementation uses an energized cell of finite dimensions to represent the energy point source. This approximation can be avoided by directly finding the effects of the energy source as a boundary condition. The proposed method transforms the Sedov problem into an outward moving radial piston problem with a time-varying velocity. A portion of the mesh adjacent to the origin is removed and the boundaries of this hole are forced with the velocities from the Sedov solution. This verification test is implemented on two types of meshes and convergence is shown. The results from the typical initial condition method and the new boundary condition method are compared.

Nomenclature

r The radial distance from the origin
r_s The radius of the shock wave at a given time
v The radial velocity of any given point
v_s The velocity immediately behind the shock wave at a given time
t The time since the initialization of the blast wave
Δr The initial radial grid spacing in the radial mesh topology
Δx The initial grid spacing in a 2D slice of the box mesh topology
λ The nondimensional ratio of radial position to the radius of the shock
θ The angle in degrees between the horizontal symmetry plane and the position vector from the origin to the cell centers (for density, pressure, or energy) or the nodes (for velocity)
ρ_z The cell center density
e_z The cell center internal energy
p_z The cell center pressure
M_z The cell mass
V_z The cell volume
$\mathbf{N}_i$ A surface area segment of a control volume surface
$\mathbf{u}_p$ The velocity of a node in the mesh
γ An equation of state parameter

1 INTRODUCTION

Analytical and computational explorations of explosion modelling have been an important area of research for many decades. Von Neumann [1], Taylor [2], and Sedov [3] all independently found a set of self-similar equations describing an idealized form of an explosion. Their simplified models use an infinitely small point source of energy as a seed. As long as the energy is large enough, this creates a strong shock that propagates outwards. Their solutions describe the self-similar equations for the evolution of state variables as the shock progresses. Because Sedov's solution was the most rigorous of his time, these self-similar equations are referred to as "Sedov solutions" in this paper.

The Sedov solution can be used to understand many real-world phenomenon involving blast waves, including the evolution of supernovas [4], detonation of high explosives, and expanding laser-heated plasmas [5]. The Sedov blast wave is also of great value as a verification problem because of the semi-analytical solution for all relevant state variables. It is possible to quantify the accuracy of a hydrodynamic approach at simulating shock waves, radial propagation of energy, and large variations in the energy. Furthermore, con-

*Corresponding author. E-mail address: nmorgan@lanl.gov (N. R. Morgan).

vergence studies can be performed to ensure that a code will continue to increase in accuracy as the resolution increases.

The traditional set-up of a Sedov blast wave simulation is an initial condition problem with a finite energy source uniformly distributed in the cell nearest the origin. The finite energy source is an approximation of the point source used with the analytic solution. The approximation of the point source as a finite source introduces a secondary error into the simulation. It has generally been assumed that the convergence rates are maintained since the error in approximating the point source and the error in the numerical discretization go to zero in the continuum limit. Nevertheless, it has been hypothesized that some simulation errors might be attributed to the finite energy source approximation [6] at finite grid resolutions. This has the possibility of making grid convergence studies difficult, especially if order of the secondary error is different than the order of the discretization error.

This paper introduces a new method for modeling the point source that eliminates this secondary error. In order to avoid using an energized cell of finite size, the computational domain was modified to remove the cell(s) adjacent to the origin. The effects of the point source can then be applied to the exposed nodes as a boundary condition. As the energy propagates outwards, the nodes on this boundary are driven by a time-varying velocity boundary condition corresponding to the semi-analytic solution. While the initial condition method would only approximate these velocities near the origin, this method applies them using the semi-analytic solution. This makes the Sedov problem equivalent to an outward moving radial piston problem in which a shock wave emanates from the origin due to an applied velocity boundary condition.

This new approach represents a significant departure from the typical methodology in at least two regards. First, the typical setup as an initial condition problem is transformed into a time-dependent boundary condition problem. The new approach verifies the ability of a hydrodynamic method to convert kinetic energy into internal energy, similar to the Noh problem [7]. Second, this approach eliminates the errors resulting from approximating the energy point source as an energy source of finite volume. This allows one to determine whether errors seen in a typical Sedov simulation (*i.e.,* the Sedov problem is run as an initial condition problem) are due to the approximation of the point source. One can then analyze how well any particular approach performs independent of the setup errors. This new approach was tested on a Lagrangian staggered grid hydrodynamic approach [8–11] and results are presented and compared to the traditional approach of using a finite energy source.

2 TEST PROBLEM METHODOLOGY

Once the cell(s) containing the origin of the blast wave has been removed, the appropriate boundary conditions must be applied to the exposed nodes. The corresponding velocity at the respective nodes can be found using the semi-analytic Sedov solution; this methodology is summarized here and explained in greater detail in the following subsections. Sedov's original solution results in a semi-analytic solution that gives a nondimensional radius, λ, and a nondimensional velocity, f. Using this similarity solution, one can then find the velocity of a particle at any position and at any time. The kinematic ordinary differential equation (ODE) relating the position and the velocity must be solved to find the vertex velocities as a function of time. The end result of this is a set of time-dependent velocity boundary conditions that can be used in a hydrodynamic code.

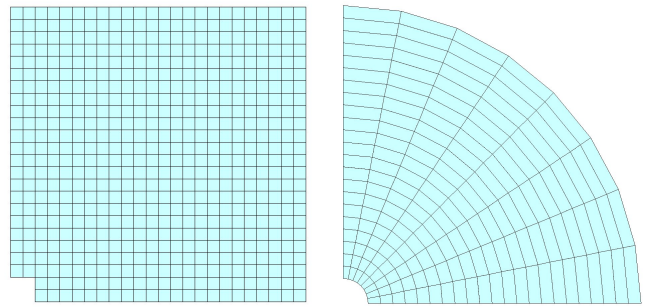

(a) Box Mesh **(b)** Radial Mesh

Fig. 1: The axisymmetric (RZ) meshes used with the new verification test problem are shown. Cell(s) are removed near the origin and the velocity boundary conditions are applied to the nodes exposed on the inner surface. For both meshes, the horizontal axis is Z and the vertical axis is R.

2.1 Mesh Modifications

Two separate types of computational domains are described in this paper. The first type corresponds to a "classical" or initial condition (IC) Sedov problem, where the blast wave is initiated by an energy source of finite dimensions. The second corresponds to the outward moving "radial piston" or boundary condition (BC) Sedov problem, where a continuous set of cells adjacent to the origin are removed (Fig. 1.).

For the velocity BC Sedov problem, the exact same computational domain is used with only one modification. A portion of the mesh next to the origin is removed; this region can be of various sizes and shapes. The aforementioned velocity boundary conditions are applied to the nodes exposed by removing the cells adjacent to the origin. The initial density and computational discretization are otherwise identical to the classical Sedov solution. Two examples of this modified computational domain can be seen in Fig. 1.

2.2 Solution to Sedov's Equations

Kamm explained a robust method for numerically solving Sedov's equations [12], which is summarized in this subsection. A more succinct treatment of the underlying equations and their analytical solution is given in the Landau and LIfshitz text [13]. The Sedov solution assumes that the fluid of interest is compressible, inviscid, and governed by the gamma-law equation of state. The most difficult portion of

the calculation is relating the integral of energy over the domain to the state variables inside the shock region. Once this integral relation is solved, the similarity solution can be found using a set of algebraic equations. These algebraic equations can be used to find nondimensional values, among which are f and λ, which are defined as:

$$\begin{aligned} f &= v/v_s \\ \lambda &= r/r_s \end{aligned} \tag{1}$$

where r is the radial distance from the origin of the blast to any defined point, r_s is the radius of the shock wave, v is the radial material velocity of the same defined point, and v_s represent the radial material velocity immediately following the shock. Other similarity variables also exist for density and pressure. These similarity variables are coupled, meaning each value of f corresponds to exactly one value of λ. Because the similarity solution involves nondimensional measures of radius and time, a function relating f and λ is valid for all positions and all times. Selecting a specific position and time corresponds to selecting a specific value of f or λ. Since λ is the radial position, it is easiest to use this as the independent variable and f as a dependent variable. Once f and λ are known for a given point, all the relevant properties (density, velocity, pressure, or internal energy) can be computed by multiplying the similarity variables by the post-shock conditions. The calculation of these similarity variables was performed using the code presented in Reference [12].

2.3 Generation of Velocity Boundary Constraints

Once the relation between radius and velocity is determined, a table of boundary conditions is generated. This table represents the velocity of each node individually as a function of time, for all times spanning the duration of the simulation. Since these boundary conditions are velocities, they are applied to those nodes exposed by removing the cell(s) at the origin. The velocity of a node can be represented as a function of the radial distance and time, or $v = g(r,t)$, where g is a function. Due to the Lagrangian motion of the simulation, this node represents a particle that must be followed throughout the time domain. This can be done by substituting the nondimensional velocity into the ODE relating position, velocity, and time:

$$dr/dt = v(r,t) = f(r,t)v_s(t) \tag{2}$$

where f is the nondimensional ratio of velocities for a given point and time and v_s is the radial material velocity immediately following the shock. From this kinematic ODE, the velocities and positions of individual nodes can be solved. In order to include these velocities in the hydrodynamic code, a table of velocity BC values is created. The same time steps were used for both the ODE solver and the table of velocity BCs for consistency purposes. As one can see from Fig. 2,

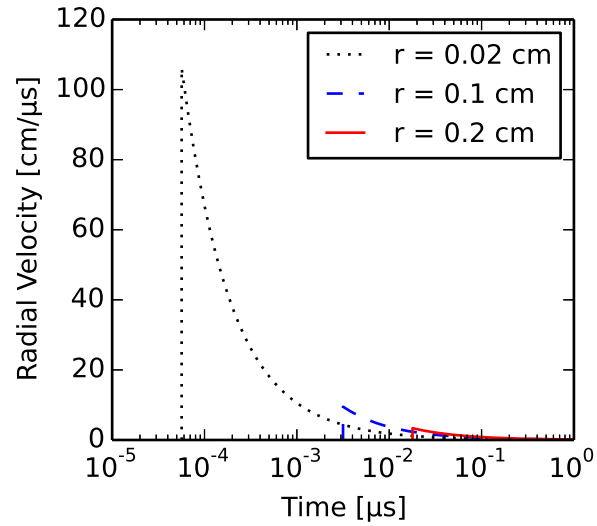

Fig. 2: A comparison of material velocities for particles at three different initial positions as a function of time. The velocity jump for a position of $r = 0.02$ cm is about two orders of magnitude larger than the jump for $r = 0.2$ cm.

the ODE is a stiff problem due to the sudden change in velocity as the shock wave passes. Several different numerical ODE solvers were considered, varying from the basic forward Euler method to the fourth-order Runge-Kutta method.

The best results were found using a method similar to that proposed by Bogacki and Shampine (hereafter referred to as BS23) [14]. The BS23 method compares a second and third-order Runge-Kutta method to estimate the error with each new time step. If the error is above a specified threshold, the step size is reduced until the error falls below the specified threshold. This method allows adaptive temporal refinement to be employed and places explicit limitations on truncation errors. The higher-order RK45 method could also be used in a similar fashion with even greater temporal accuracy.

For the implementation described in Section 3, this table of velocities is used by the hydrodynamics code. The code interpolates among the tabular values to find the velocity at each time step using a cubic spline. The table is also very finely resolved to minimize any interpolation errors. The following two subsections address the accuracy of calculating the velocity boundary conditions.

2.4 Convergence of ODE Solvers

Forward Euler and Runge-Kutta methods were investigated using several time stepping-schemes for solving the ODE in Eq. 2. These solvers were compared using a hole size of 0.02 cm, since this size has the sharpest discontinuity of all the hole sizes considered (Fig. 2). The relative error of these solvers is shown in Fig. 3. The relative error incurred by the ODE solver was found to be highly dependent on the type of time step used. This can easily be seen

by comparing the differences between logarithmic temporal spacing and the quadratic temporal spacing for the classical fourth-order Runge-Kutta method. From Fig. 3 it can be seen that the BS23 method has the smallest error. Even though this method employs a third-order Runge-Kutta solution, the adaptive time step size gives it a lower relative error than of the fourth-order Runge-Kutta schemes. This same technique could be applied with other higher-order adaptive algorithms, including RK45, with even greater temporal accuracy. Based on the results shown, a table with 2000 values or more is recommended for the velocity BC table. The numerical generation of this table adds a maximum possible relative error on the order of 1E-8 to the solution. This error falls well below the relative error of the hydrodynamic approach for reasonable mesh resolutions.

A second test was used to further assess the accuracy of the BS23 solver. The second test evolves a uniformly spaced radial mesh to t = 1 μs by solving the ODE in Eq. 2, and a comparison is made to the semi-analytic Sedov solution for the density and velocity at this time. Since the mesh is Lagrangian (mass is constant for all time), the final density can be calculated by dividing the initial cell mass by the final cell volume. This density is an average density. This solution solely relies on the solution of the kinematic ODE 2, so it is a good test of whether these velocity BCs can accurately predict the final density distribution. The calculated density profile and velocity profile are plotted versus the analytic solutions in Fig. 4. As seen in the figure, the BS23 method reproduces the semi-analytic Sedov density and velocity profiles at t = 1 μs. It might be helpful to note that there is a cell that bridges the shock wave. The properties are very different on both sides of the cell so the average density in this cell cannot match the exact properties of the Sedov semi-analytic solution. This sort of behavior is to be expected.

2.5 Summary of Necessary Steps

The following is a summary of the steps taken to run a verification test using the new BC verification approach. An example of typical results is shown in Fig. 5, where the density fields and meshes for the IC and BC approaches are shown side by side.

1. Determine the state variables to be used (blast energy, initial density distribution, initial pressure, and gamma).
2. Remove a section of the mesh adjacent to the origin.
3. Determine the radial distance from the origin to each vertex on the exposed boundary.
4. Solve the semi-analytic equations described by Kamm to find the similarity solution relating f and λ [12].
5. For each vertex, determine the starting time when the shock will arrive.
6. Calculate the post-shock conditions as functions of time using gas dynamics relations.
7. For each vertex, use the initial position, starting time, post-shock conditions, and solution for f and λ to solve the ODE for r, v, and t.
8. Use the time varying radial velocity as a boundary condition.

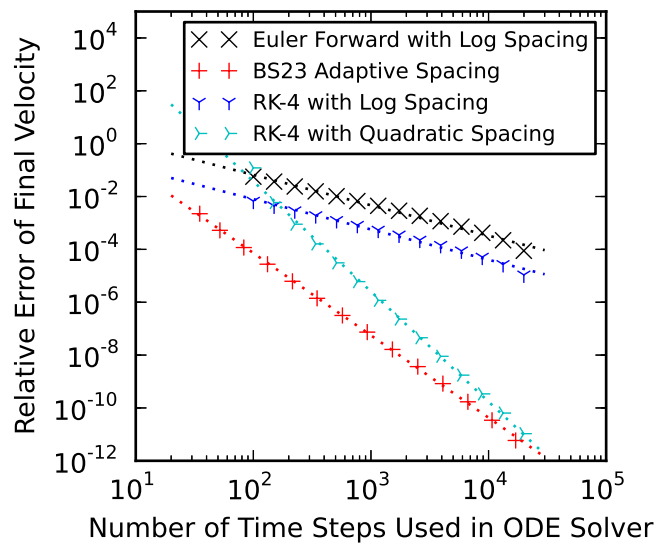

Fig. 3: Convergence rates of the four ODE solvers are presented. The forward Euler with a logarithmic spacing, fourth-order Runge-Kutta with logarithmic spacing, fourth-order Runge-Kutta with quadratic spacing, and the BS23 adaptive time-stepping method were studied.

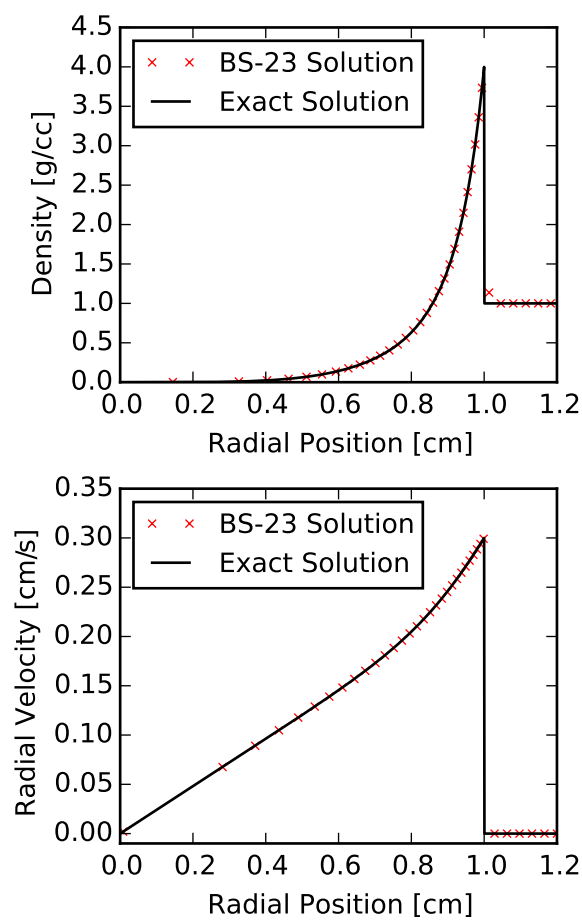

Fig. 4: Comparison of density and velocity profiles generated by the BS23 solver with the analytic solution

3 TEST IMPLEMENTATION

The following sections discuss the application of the new BC verification approach to a Lagrangian hydrodynamic approach. The setup parameters are described and the errors in each implementation approach (IC and BC) are presented. The convergence results and plots are provided in Section 4.

3.1 Description of Lagrangian Hydrodynamic Algorithm

The new BC verification approach is applied to a finite volume staggered grid hydrodynamics (SGH) approach [8–11]. The SGH approach solves the governing equations on two staggered meshes. The conservation of momentum is solved on a control volume around a node. The density, pressure, internal energy, and other state variables are defined at the cell centers. The evolution of the internal energy is solved on the cell boundary using a compatible discretization described in [8, 9]. In order to better capture the changes in state variables across the shock, the Godunov-like approach suggested in [11] was used. With this approach, a multidirectional Riemann-like problem is solved at the cell center. The inputs to the Riemann problem are velocity, which are calculated by projecting the nodal values to the cell center with a linear Taylor-Series expansion. The gradients in the Taylor-Series are limited [11] to minimize spurious oscillations near shocks. This approach is second-order accurate on smooth flows and first-order accurate at shocks. One advantage of this method is that it is very robust against mesh instabilities such as hourglass modes and chevron modes.

3.2 Computational Domain and State Variables

The Sedov blast wave can be planar, cylindrical, or spherical. The problems simulated in this paper are strictly spherical blast waves. The calculations are performed using 2D RZ axisymmetric coordinates. In order to fully examine the Sedov verification test, two types of meshes were examined for both the IC and the BC verification approaches. Fig. 1 shows the two types of axisymmetric meshes, which are termed box and radial. These terms refer specifically to the mesh topology. In this paper, a square hole is used for the box mesh and a circular hole is used for the radial mesh. Three different hole lengths were considered: 0.02 cm, 0.1 cm, and 0.2 cm. The outer bounds of the computational domain was set to 1.2 cm x 1.2 cm.

The ratio of specific heats (gamma) was set to 5/3, but other values of gamma could be used. The initial density was set to 1.0 g/cc everywhere. For the IC calculations, the extensive source internal energy was set to 0.493390 Mbar g/cc. This energy was chosen so that the shock would be located at a radius of 1.0 cm at a time of 1.0 μs. The specific source internal energy used for the IC method is calculated by dividing by the mass in the source cell. The source energy must be scaled to account for the symmetry conditions in the z-direction. The boundary velocity applied in the BC approach was calculated for an extensive source internal energy equal to 0.493390 Mbar g/cc.

4 CONVERGENCE OF LAGRANGIAN SGH

The Lagrangian SGH method was observed to converge at approximately first-order to the exact solution using the BC verification approach. The calculated density, pressure, velocity, and internal energy profiles are plotted in Fig. 6 for 3 resolutions using a radial mesh topology. As shown, the calculations are in reasonable agreement with the analytic solution and the agreement improves as the mesh resolution increases. Small overshoots are present in the pressure and density profiles at the shock front. These small overshoots are created by errors in the cell volume evolution. The density of a cell, ρ, is calculated using

$$\rho_z = \frac{M_z}{V_z} \tag{3}$$

where M_z is the cell mass and V_z is the cell volume at some time t. The discrete rate of change of the cell volume is given by,

$$\frac{1}{V_z}\frac{\Delta V_z}{\Delta t} = \nabla_z \cdot \mathbf{u} = \frac{1}{V}\sum_{i \in z} \mathbf{N}_i \cdot \mathbf{u}_p \tag{4}$$

where $\mathbf{u}_p$ is the velocity of the nodes and $\mathbf{N}_i$ is a surface area segment of the cell surface connected to the node, p. The summation is over all surface area segements in the cell, $i \in z$. An excessively large jump in velocity across the cell (i.e., $\nabla_z \cdot \mathbf{u}$) will translate into overshoots in the density field. Using a more aggressive limiter on the gradients in the velocity reconstruction will smooth the velocity profile, which will smooth the density field, but this will also degrade the accuracy. Fig. 6 illustrates that this Lagrangian approach can capture most of the velocity jump at the shock front in a single cell, which translates into a small overshoot in density that affects the pressure field through the equation of state, $p = \rho(\gamma - 1)e$.

Convergence studies were performed using both the radial and box mesh topologies. The convergence was calculated using an L1 error norm weighted by the volume of each cell. Despite the common usage of the L2 error norm, the L1 error norm is usually a more stringent test and is especially appropriate for problems containing shocks or solutions with large derivatives. The L1 error norm for a quantity of interest, U, is calculated using the formula:

$$L_U^1 = \frac{\sum_{j \in \mathcal{R}} (V_j |U_j - U_{exact}|)}{\sum (V_j)} \tag{5}$$

where V_j is the volume of the respective control volume (*i.e.,* cell or nodal) and $\mathcal{R}$ is the problem domain. This is the same error normalization used to thoroughly investigate the error involved in CCH and SGH methods in [15]. All of the convergence plots use this error normalization.

The convergence of Lagrangian SGH L1 errors using the BC approach is presented in Fig. 7. As demonstrated, the L1

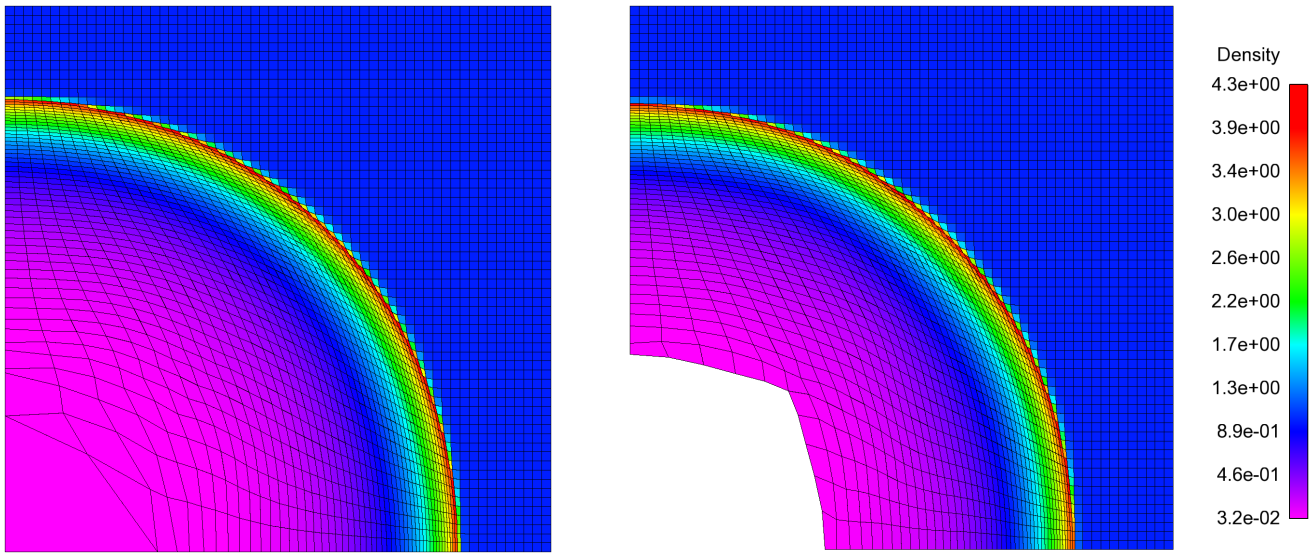

(a) Initial Condition Method

(b) Boundary Condition Method

Fig. 5: The density and mesh are shown for the IC and BC approaches using a box mesh topology

errors shrink monotonically as the cell size decreases. Convergence rates were determined by the common least squares fit to the assumed single-term power-law form. These convergence rates and the correlation coefficients can be seen in Tables 1 and 2. The correlation coefficients for the two larger holes are all above 0.978, signifying a predictable convergence with no extraneous grid-dependent errors. The magnitude of the L1 errors in the final solution are a function of the hole size at the origin. The larger hole had a smaller L1 error compared to the smaller hole. This difference is attributed to the large magnitudes of gradients and higher derivatives of velocity and energy near the origin at very small times. The relative scales in the velocity for various initial radii can be seen in Fig. 2. As the blast wave spreads out from the origin, the velocity behind the shock slows from approximately 100 cm/μs at $r = 0.02$ cm to approximately 4 cm/μs at $r = 0.2$ cm. Even small relative errors near the origin can lead to numerical errors that are 1-2 orders of magnitude larger than errors far from the origin. The convergence rates are similar for all hole sizes.

In general, grid convergence testing is only valid for resolutions dense enough to be within the asymptotic range of convergence [16]. At least two of the coarsest meshes appear to fall outside this range where the single-term power-law is valid. The L1 the error did not decrease significantly at the coarsest mesh resolutions for the radial mesh topology with a hole size of $r = 0.02$ cm (see Fig. 8). It is not too surprising that significant resolution is required to capture an initial velocity of order 100 cm/μs. Once the resolution exceeds the threshold (appearing just beyond 1/2 of the hole size) the L1 error begins to decrease at about the same convergence rate as the other hole sizes, with correlation coefficients of 0.993 and 0.996 for the density and pressure errors respectively on a radial mesh. Including the coarsest two resolutions makes the correlation through the L1 error data to become 0.935 and 0.950 for the density and pressure errors. These lower correlation coefficients suggest that a single-term power-law does not completely describe the convergence rate for small hole sizes at coarse mesh resolutions.

Table 1: Comparison of the L1 density error as a function of various hole sizes (for the BC Method)

	Box Mesh		Radial Mesh	
Hole Size	Order	R^2	Order	R^2
0.02 cm	0.77	0.989	0.93	0.993
0.10 cm	0.80	0.993	1.10	0.978
0.20 cm	0.85	0.999	1.08	0.994

Table 2: Comparison of the L1 pressure error as a function of various hole sizes (for the BC Method)

	Box Mesh		Radial Mesh	
Hole Size	Order	R^2	Order	R^2
0.02 cm	0.79	0.989	1.00	0.996
0.10 cm	0.82	0.995	1.18	0.988
0.20 cm	0.83	0.999	1.06	0.996

4.1 Results from Radial and Box Mesh Topologies

The BC verification test was used to quantity the numerical errors and rate of converge of a Lagrangian SGH ap-

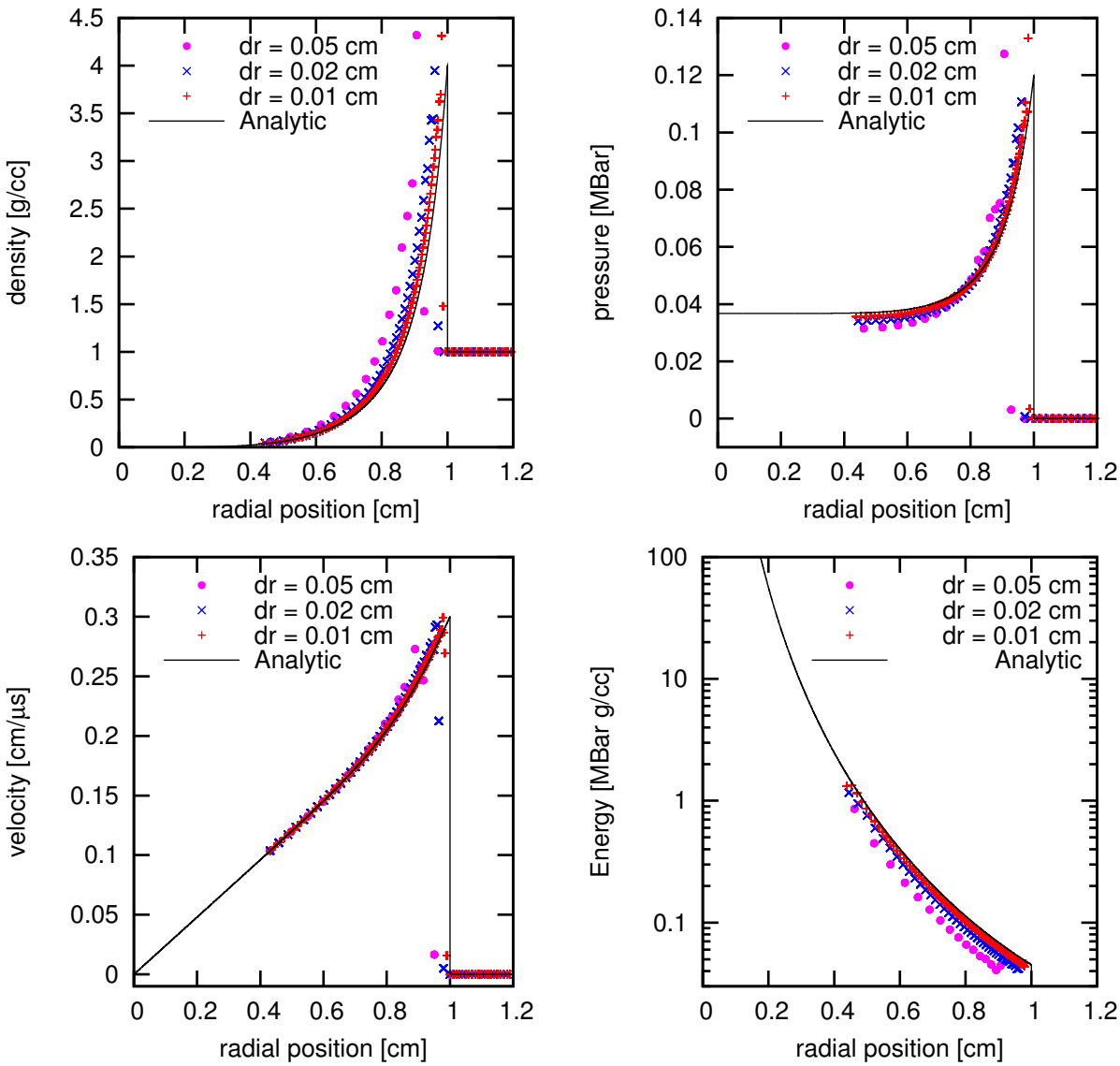

Fig. 6: The plots of density, pressure, velocity, and internal energy for various mesh resolutions are provided using a radial mesh. These results were generated using the new BC verification approach. The calculations are approaching the analytic solution as the mesh resolution increases. Convergence plots are provided in Figs. 7 and 8.

proach. The error regression data is plotted in Figs. 7 and 8. In these plots, the "initial edge length" (the abscissa in the graphs) represents different quantities in the box and radial meshes (Fig. 1). For the box mesh, it is simply the initial grid spacing, dx. For the radial mesh, it is the grid spacing along the radial cell divisions (as opposed to the angular spacing) and is denoted as dr. Despite the similarity in these two scales, the distribution of cells volumes will generally not be the identical, even for $dx = dr$. Therefore, the errors are not expected to be the same even at the same initial edge length.

The results of this verification test can be used to explore the errors inherent in a numerical scheme. For example, Fig. 9 shows the absolute errors in the box mesh topology as a function of both the radial position and the angle, where θ is the angle in degrees between the horizontal symmetry plane and the position vector from the origin to the cell centers (for density, pressure, or energy) or the nodes (for velocity). According to this definition, $\theta = 0°$ corresponds to the horizontal axis and $\theta = 90°$ corresponds to the vertical axis. From this plot, it can be seen that there is a definite dependence upon θ.

5 Comparison between the IC the BC Approaches

A plot of the deformed mesh and the density distribution was shown for both the IC (old) and the BC (new) verification approaches in Fig. 5. The L1 errors for the IC and BC approaches are plotted in Figure 10 using both radial and box mesh topologies. The results from the BC approach correspond to a hole size of 0.2 cm. For the IC approach, the errors are very similar for a box and a radial mesh topol-

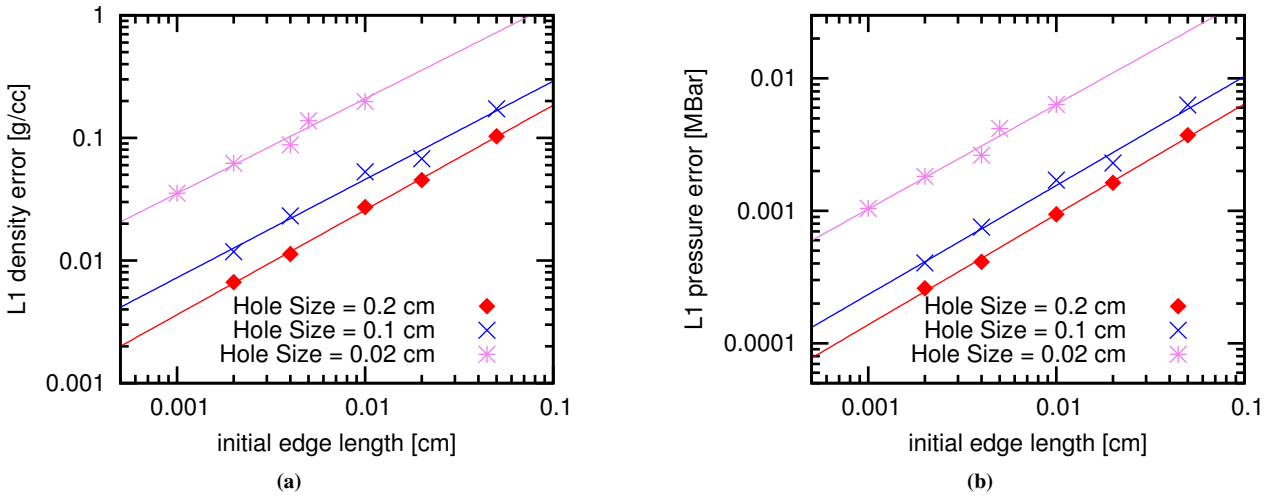

Fig. 7: Convergence plots are shown for the a) density and b) pressure fields for the BC approach using a box mesh topology. The initial edge length is dx(t=0). The holes are a square with lengths = 0.02 cm, 0.1 cm, and 0.2 cm respectively. For the density, the order of convergence for the different hole sizes was 0.77, 0.80, and 0.85. For pressure, the orders of convergence were 0.79, 0.82, and 0.83.

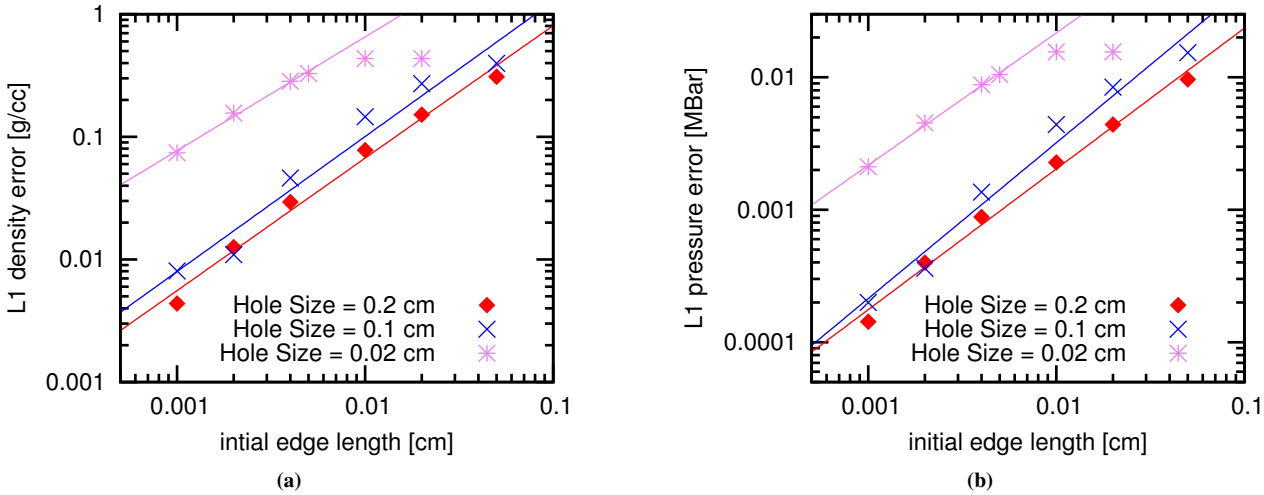

Fig. 8: Convergence plots are shown for the a) density and b) pressure fields for the BC approach using a radial mesh topology. The initial edge length is dr(t=0). The radii of the holes are 0.02 cm, 0.1 cm, and 0.2 cm respectively. For the density, the order of convergence for the different radii was 0.93, 1.10, and 1.08. For pressure, the orders of convergence was 1.00, 1.18, and 1.06.

ogy. The Lagrangian SGH approach using the IC and BC approaches is converging at a rate close to 1, which is the expected convergence rate [11, 15]. However, the magnitude of the numerical errors are slightly higher with the BC approach.

The absolute value of errors for the radial mesh and box mesh are plotted in Figures 11 and 12 respectively as a function of the radius to help understand the larger error with the BC approach. Error plots are provided for density, pressure, velocity, and internal energy. The cusps in the plots correspond to places where the numerical solution crossed the exact solution. From these figures it can be observed that the errors in density and energy are close in value for both the IC and the BC approaches near the origin. However, the results from using the IC and BC approaches differ in how the energy and density propagates through the mesh. Further away from the origin, the BC method results in larger errors than those from the IC approach. It should be noted that these errors are not attributed to the verification test itself, since any errors involved in the setup of the test are many orders of magnitude smaller than the errors in the results. The errors are instead attributed to the hydrodynamic method. The larger errors seen in this BC test are consistent with other velocity-driven verification test problems, such as

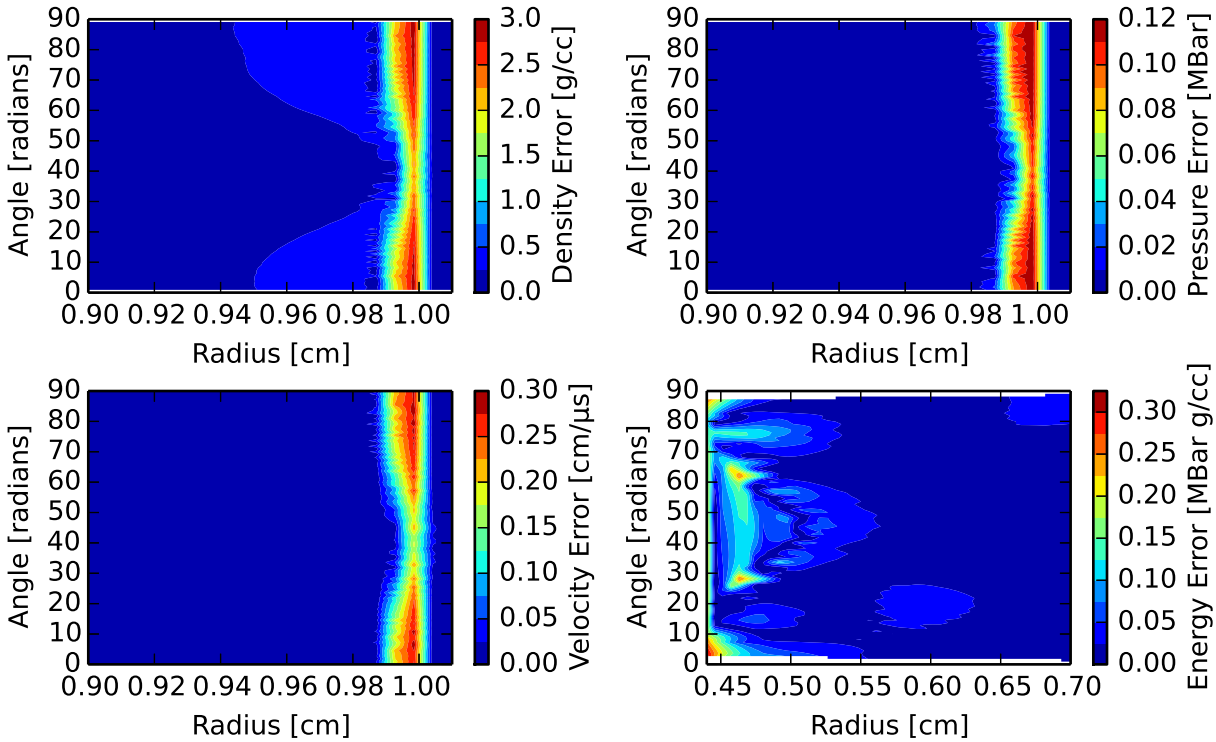

Fig. 9: Absolute value of the errors as a function of radius and angle, using the box mesh topology, a grid spacing of dx=0.02 cm, and an initial hole size of 0.02 cm

Table 3: Characteristics of the least squares regressions for the L1 density error for the IC and the BC method are presented. A hole size 0.2 cm is used for the BC method.

Setup	Order	R^2
IC, Box Mesh	0.91	0.994
IC, Radial Mesh	0.74	0.995
BC, Box Mesh	0.85	0.999
BC, Radial Mesh	1.08	0.994

Table 4: Characteristics of the least squares regressions for the L1 pressure error for the IC and the BC method are presented. A hole size 0.2 cm is used for the BC method.

Setup	Order	R^2
IC, Box Mesh	0.85	0.995
IC, Radial Mesh	0.92	0.997
BC, Box Mesh	0.83	0.999
BC, Radial Mesh	1.06	0.996

Noh [7]. Hydrodynamic methods can have problems converting kinetic energy to internal energy. The verification test proposed in this paper serves to illuminate such weaknesses. This test also allows researchers to check the ability of an approach to respond to rapid changes in boundary conditions. The same principles shown in this paper could be extended to other verification tests to check the response of an approach to various types of dynamic boundary conditions.

6 CONCLUSION

A new approach for the Sedov verification test was presented. The approach models the Sedov blast wave as an outward moving radial piston problem with spatially and temporally varying velocity boundary conditions. This corresponds to a shift from an initial condition (IC) problem, where energy is deposited in a cell, to a boundary condition (BC) problem where the boundaries are moved. The applied velocity boundary conditions correspond to the velocity from the Sedov semi-analytical solution, so this new approach accurately captures the effect of the energy point source. The test problem is implemented by excluding a portion of the mesh near the origin (termed a hole) and then applying the time-varying velocity boundary conditions to the nodes on the inner surface of the mesh.

The new approach was implemented and used to verify a Lagrangian Godunov-like staggered grid hydrodynamic method [11]. Convergence studies were performed using the new BC verification approach on two types of meshes - a box

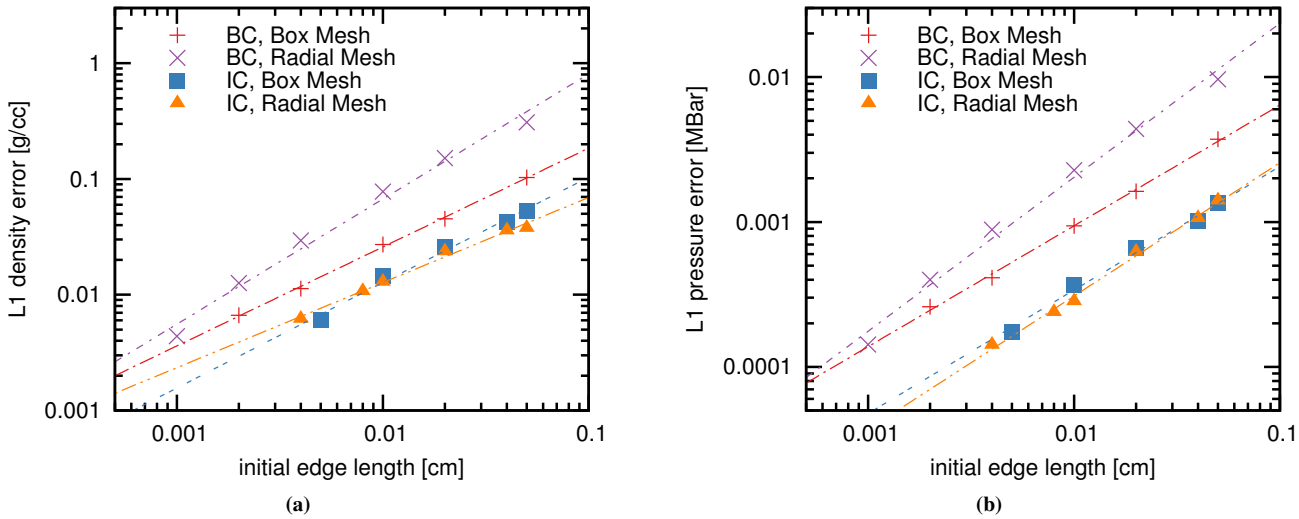

Fig. 10: Comparison of the IC and BC verification approaches using box and radial mesh topologies. The errors represented are (a) L1 density error and (b) L1 pressure error. The initial edge length for the box mesh is dx and for the radial mesh is dr. The hole size is 0.2 cm for the BC calculations. The order of convergence and correlation coefficients are provided in Table 3 and 4.

mesh and a radial mesh respectively. For a box mesh, convergence rates in the L1 norm were observed between 0.77 and 0.85 for density, and between 0.79 and 0.83 for pressure. For a radial mesh, convergence rates in the L1 norm were observed between 0.93 and 1.10 for density, and between 1.00 and 1.18 for pressure. The radial mesh had better convergence rates than a box mesh. The convergence rates from the BC approach were compared to those from the IC approach. For a polar mesh, the BC approach had a better rate of convergence than the IC approach. For a box mesh, the BC approach had convergence rates slightly less than the IC approach.

The new BC approach offers another way to verify a hydrodynamic method using a classical test problem. This test can be used to verify that the secondary errors in the IC Sedov test, introduced through the use of an energized region of finite size, are relatively small. Furthermore, this test also stands as an independent measure of a hydrodynamic method's ability to capture time-dependent velocity boundary conditions. The boundary condition approach presented in this paper could potentially be applied to Eulerian verification test problems. The concept of converting initial condition test problems to boundary driven problems could potentially be applied to a wider range of verification tests.

Acknowledgements

We gratefully acknowledge the support of the Advanced Scientific Computing (ASC) program at Los Alamos National Laboratory. We thank Jim Kamm for his input and help with this work. We also acknowledge the efforts of Scott Runnels in organizing the LANL Computational Physics Summer Workshop, under which the research for this paper was conducted. The Los Alamos unlimited release publication number is LA-UR-15-27276.

References

[1] von Neumann, J., 1963. "The point source solution". In *John von Neumann: Collected Works*, A. Taub, ed., 6 ed. Permagon Press, Elmsford, N.Y., pp. 219–237.

[2] Taylor, G., 1950. "The formation of a blast wave by a very intense explosion". *Proceedings of the Royal Society of London. Series A, Mathematical and Physical Sciences*, pp. 159–174.

[3] Sedov, L. I., 1959. *Similarity and dimensional analysis in mechanics*. Academic Press, New York, N.Y.

[4] Chevalier, R. A., 1976. "The hydrodynamics of type II supernovae". *Journal of Astrophysics*, pp. 207–872.

[5] Leonard, T. A., and Mayer, F., 1975. "Helium blast-wave measurements of laser-heated microshell targets". *Journal of Applied Physics,* **46**(8), pp. 3562–3565.

[6] Kamm, J., 2000. Evaluation of the Sedov-von Neumann-Taylor Blast Wave Solution. Tech. Rep. LA-UR-00-6055, Los Alamos National Laboratory, Los Alamos, NM.

[7] Noh, W. F., 1987. "Errors for calculations of strong shocks using an artificial viscosity and an artificial heat flux". *Journal of Computational Physics,* **72**(1), pp. 78–120.

[8] Burton, D. E., 1994. "Multidimensional Discretization of Conservation Laws for Unstructured Polyhedral Grids". In 2nd International Workshop on Analytical Methods and Process Optimization in Fluid and Gas Mechanics.

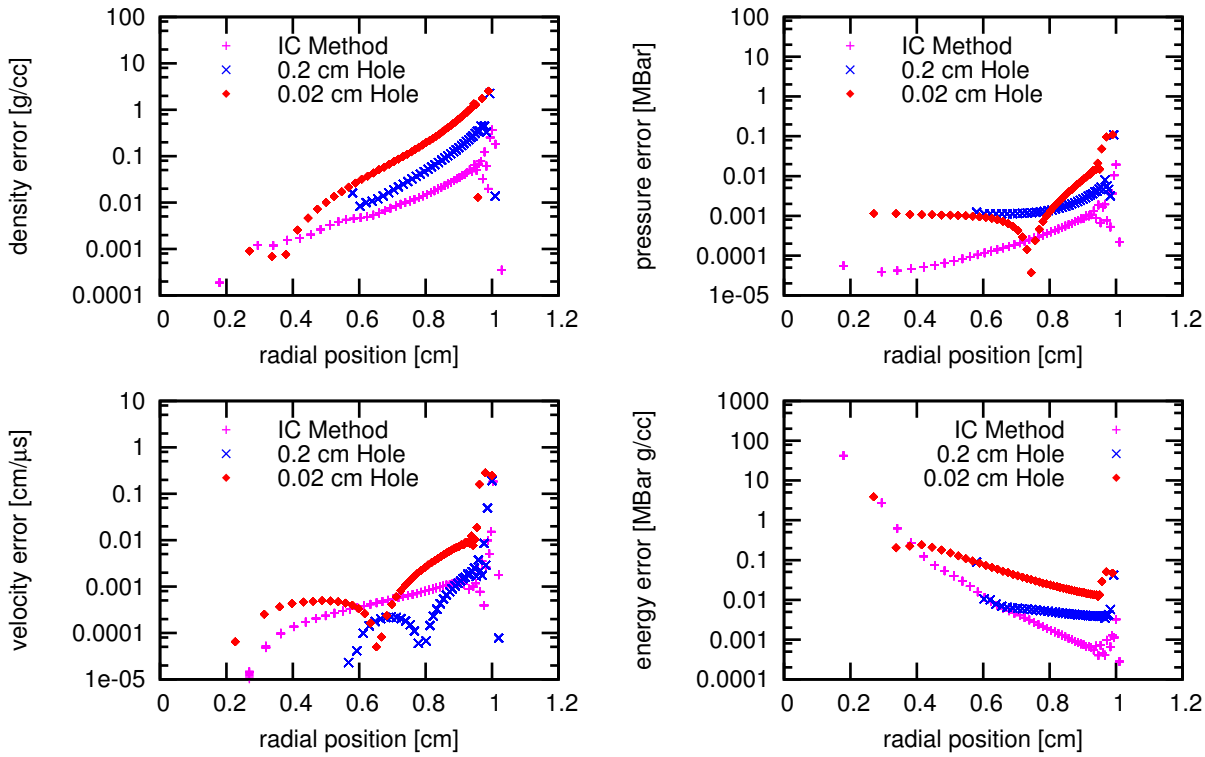

Fig. 11: Absolute values of the errors are compared for the IC method and the BC method using the radial mesh. For the BC method, results for hole sizes of 0.02 cm (red points) and 0.2 cm (blue points) are shown. The initial edge length of the mesh (dr) is 0.02 cm for all calculations shown.

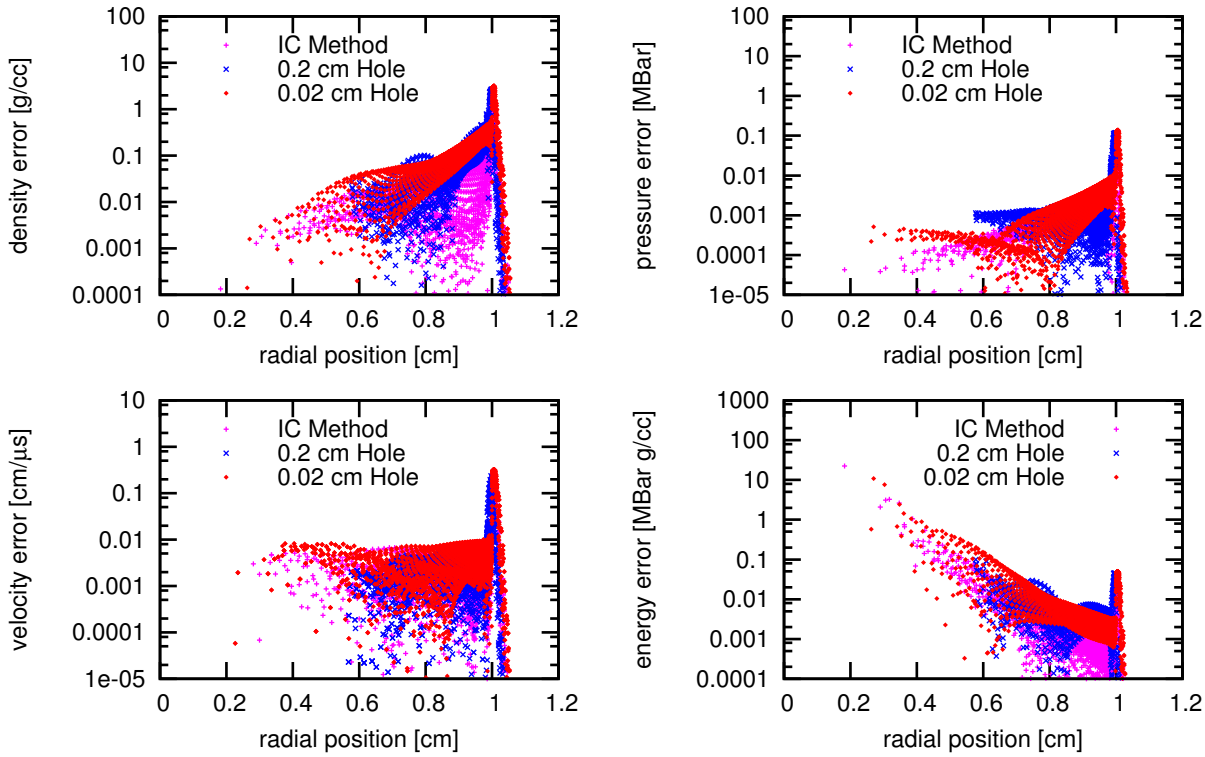

Fig. 12: Absolute values of the errors are compared for the IC method and the BC method using the box mesh. For the BC method, results for hole sizes of 0.02 cm (red points) and 0.2 cm (blue points) are shown. The initial edge length of the mesh (dx) is 0.02 cm for all calculations shown.

[9] Caramana, E., Burton, D., Shashkov, M., and Whalen, P., 1998. "The construction of compatible hydrodynamic algorithms utilizing conservation of total energy". *Journal of Applied Physics,* **146**, pp. 227–262.

[10] Burton, D. E., 2008. Lagrangian Hydrodynamics in the FLAG Code. Tech. rep., Los Alamos National Laboratory.

[11] Morgan, N. R., Lipnikov, K. N., Burton, D. E., and Kenamond, M. A., 2014. "A Lagrangian staggered grid Godunov-like approach for hydrodynamics". *Journal of Computational Physics,* **259**, pp. 568–597.

[12] Kamm, J. R., and Timmes, F. X., 2007. On efficient generation of numerically robust Sedov solutions. Tech. Rep. LA-UR-07-2849, Los Alamos National Laboratory, Los Alamos, NM.

[13] L. D. Landau, E. M. L., 1959. *Fluid Mechanics*. Pergamon Press Ltd., Elmsford, New York, pp. 392–396.

[14] Bogacki, P., and Shampine, L., 1989. "A 3(2) Pair of Runge-Kutta Formulas". *Appl Math Lett,* **2**(4), pp. 321–325.

[15] Doebling, S., 2014. Impact of numerical treatment of shocks on verification assessment of the FLAG Lagrangian hydrodynamics code using the Sedov problem. Tech. rep., Los Alamos National Laboratory.

[16] Roache, P. J., 1998. "Verification of codes and calculations". *AIAA journal,* **36**(5), pp. 696–702.